AFRL-RD-PS-
TP-2024-0003

CLOSELY SPACED OBJECT DETECTION UTILIZING SPATIAL INFORMATION IN SPECTROASTROMETRIC OBSERVATIONS

Justin Fletcher, et al.

16 February 2022

Technical Paper

AIR FORCE RESEARCH LABORATORY
Directed Energy Directorate
3550 Aberdeen Ave SE
AIR FORCE MATERIEL COMMAND
KIRTLAND AIR FORCE BASE, NM 87117-5776

REPORT DOCUMENTATION PAGE

1. REPORT DATE	2. REPORT TYPE	3. DATES COVERED	
		START DATE	END DATE
16 February 2022	Paper		

4. TITLE AND SUBTITLE

CLOSELY SPACED OBJECT DETECTION UTILIZING SPATIAL INFORMATION IN SPECTROASTROMETRIC OBSERVATIONS

5a. CONTRACT NUMBER	5b. GRANT NUMBER	5c. PROGRAM ELEMENT NUMBER
5d. PROJECT NUMBER	**5e. TASK NUMBER**	**5f. WORK UNIT NUMBER**
		No associated work unit number

6. AUTHOR(S)

Justin Fletcher J. Zachary Gazak Zachary Funke
Ryan Swindle Matthew Phelps

7. PERFORMING ORGANIZATION NAME(S) AND ADDRESS(ES)

Air Force Research Laboratory
550 Lipoa Parkway
Kihei, HI 96753

8. PERFORMING ORGANIZATION REPORT NUMBER

AFRL-RD-PS-TP-2024-0003

9. SPONSORING/MONITORING AGENCY NAME(S) AND ADDRESS(ES)	10. SPONSOR/MONITOR'S ACRONYM(S)	11. SPONSOR/MONITOR'S REPORT NUMBER(S)
	AFRL/RDSM	AFRL-2022-1183

12. DISTRIBUTION/AVAILABILITY STATEMENT

Distribution A:
Approved for public release; distribution is unlimited. Public Affairs release approval # AFRL-2022-1183

13. SUPPLEMENTARY NOTES

14. ABSTRACT

The detection of closely spaced artificial satellites informs tactical decision making in a high risk scenario in the space domain. In regimes where spatial information is lost (ground observations of small or distant satellites), spectroastrometry simulations have demonstrated the potential to detect the presence of multiple objects down to 0".05–ten meters at geostationary orbit–using a medium resolution optical spectrograph on a large aperture telescope.1 This technique falls into the growing field of learned space domain awareness: leveraging convolutional neural networks to rapidly infer tactical information from complex, non-intuitive data. In this work we present a field rotation nodding technique that removes the need for a priori knowledge of the closely spaced object on sky orientation. We discuss modifications to an optical spectrograph necessary to perform this technique. We present simulated bounds on the effectiveness of spectroastrometry for the detection of closely spaced objects.

15. SUBJECT TERMS

Closely spaced objects, spectroscopy, spectroastrometry, space domain awareness

16. SECURITY CLASSIFICATION OF:			17. LIMITATION OF ABSTRACT	18. NUMBER OF PAGES
a. REPORT	b. ABSTRACT	C. THIS PAGE		
Unclassified	Unclassified	Unclassified	SAR	14

19a. NAME OF RESPONSIBLE PERSON	19b. PHONE NUMBER *(Include area code)*
Justin Fletcher	

PREVIOUS EDITION IS OBSOLETE.

STANDARD FORM 298 (REV. 5/2020)
Prescribed by ANSI Std. Z39.18

Closely Spaced Object Detection utilizing Spatial Information in Spectroastrometric Observations

J. Zachary Gazak[a], Ryan Swindle[a], Zachary Funke[b], Matthew Phelps[a], and Justin Fletcher[a]

[a]United States Space Force Space Systems Command
[b]Air Force Research Laboratory

ABSTRACT

The detection of closely spaced artificial satellites informs tactical decision making in a high risk scenario in the space domain. In regimes where spatial information is lost (ground observations of small or distant satellites), spectroastrometry simulations have demonstrated the potential to detect the presence of multiple objects down to $0''.05$–ten meters at geostationary orbit–using a medium resolution optical spectrograph on a large aperture telescope.[1] This technique falls into the growing field of *learned* space domain awareness: leveraging convolutional neural networks to rapidly infer tactical information from complex, non-intuitive data. In this work we present a field rotation nodding technique that removes the need for a priori knowledge of the closely spaced object on sky orientation. We discuss modifications to an optical spectrograph necessary to perform this technique. We present simulated bounds on the effectiveness of spectroastrometry for the detection of closely spaced objects.

Keywords: Closely spaced objects, spectroscopy, spectroastrometry, space domain awareness

1. INTRODUCTION

The identification of closely spaced object (CSO) scenarios within increasingly congested orbital regimes above Earth provide opportunities for space traffic controllers to intervene in protection of on orbit assets. Further, the characterization of CSO scenarios provides information useful for monitoring planned rendezvous and proximity operations (RPOs) from the ground.

Unfortunately, atmospheric turbulence and the inextricable connection between angular resolution and the size of a telescope's primary optic makes directly imaging multiple objects within small angular separations difficult when not impossible. Such methods require exquisite adaptive optics systems with laser propagated pseudo stars on large aperture telescopes.

Two techniques with long histories in the astronomy community proffer passive identification and characterization of CSO scenarios well within the atmospheric seeing disk and down to the physical limits of diffraction without the need for adaptive optics. These solutions work by side stepping the statistical challenges of direct imaging, either by exploiting similarities in short exposure speckle patterns (speckle interferometry), or by extracting astrometric measurements from position spectroscopy (spectroastrometry). In this work we continue the development of spectroastrometry for closely spaced object detection in the field of space domain awareness.

Spectroscopically distinct objects falling within the seeing disk of a ground-based telescope will exhibit a wavering in the centroid of spatial point spread function across wavelength. This phenomenon creates a *position spectrum* which astronomers have used to measure the flux distribution between otherwise unresolvable targets.[2,3] In this paper we describe a litmus test for the presence of close companions to on sky assets and characterization of the companion using that same spectroastrometric position spectrum.

The main contributions of this work include:

- A thorough investigation of spectroastrometry as a closely spaced object detection method for space domain awareness, significantly expanding the realism of previous work.[1]

J.Z.G: jonathan.gazak.1.ctr@us.af.mil
J.F.: justin.fletcher.14.ctr@us.af.mil

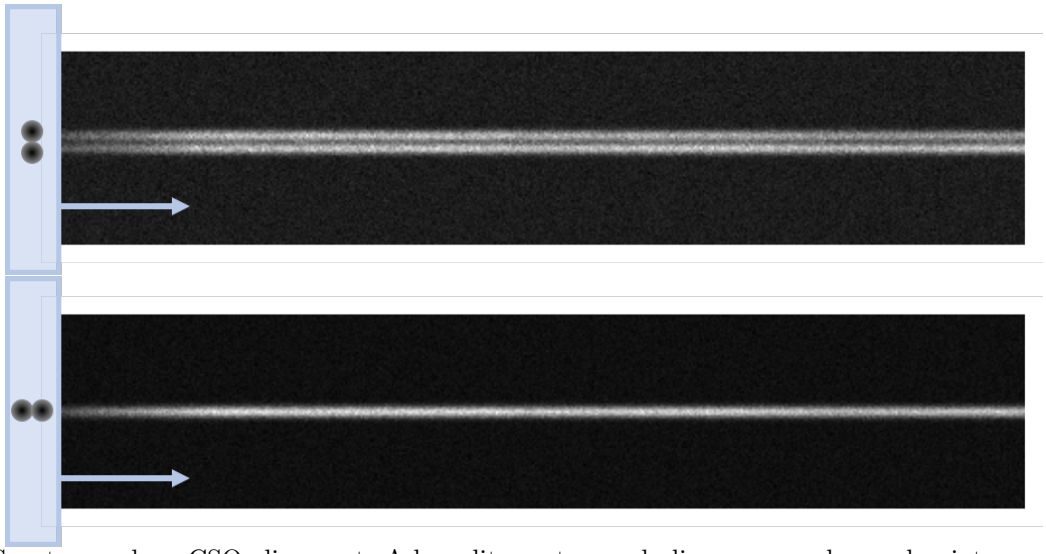

Figure 1: Spectrograph vs CSO alignment. A longslit spectrograph disperses an observed point spread function along the horizontal axis perpendicular to the observing window, as denoted by the light blue box and arrows. This alignment has a strong effect on the signal of the position spectrum in a CSO scenario. This plot demonstrates alignments on an example frame of equally bright objects with large separation (zero delta magnitude, 150 meters separation at geostationary orbit). This is done for visualization purposes. In a real scenario, such a large separation between such similar objects would not require an advanced CSO discrimination technique. **Top panel; ideal alignment**. When the observing window is perfectly aligned with the CSO geometry, the dispersed spectra are maximally separated such that the position spectrum is maximized. **Bottom panel; destructive alignment**. If the observing window is instead perpendicular to the CSO geometry, the object spectra fall on top of one another, and the position spectrum between them is entirely destroyed.

- Introduction of a mission planning framework in the form of *mission space* vocabulary allowing communication and comparison of inter-technique performance in different regimes regardless of differences in data type.

2. RELATED WORKS

2.1 Deep Learning for Space Domain Awareness

In fields driven by scientific imagery—which tend to be high contrast with often perverse noise structures—the development of first principled techniques which draw on theoretical physical knowledge to extract relevant information is often out of reach. This may be because the physics is too stochastic (reflection spectroscopy[4–6]), or because noise and feature structures too complex for hand tuned algorithms (object detection,[7] reconstruction of high resolution imagery,[?,?] and segmentation of satellites.[?] In these examples, solutions learned from high contrast scientific imagery solve problems faster and more effectively than physics based methods.

2.2 Spectroastrometry

The term "spectroastrometry" was introduced in 1998 and its application to binary stars and active galactic nuclei demonstrated on standard spectrograph hardware was demonstrated.[2] In that work, spectroastrometry is described as *position spectroscopy*, in that positional differences between different sources are processed into their spectra. We find this terminology best elucidates the complex data representation and describes how positional information approaching a telescope's diffraction limit can be extracted regardless of atmospheric seeing conditions.

Unlike techniques like adaptive optics—requiring advanced optics, or speckle interferometry—requiring short exposure times and thus large apertures, spectroastrometry is well suited to mass proliferation on small telescopes.

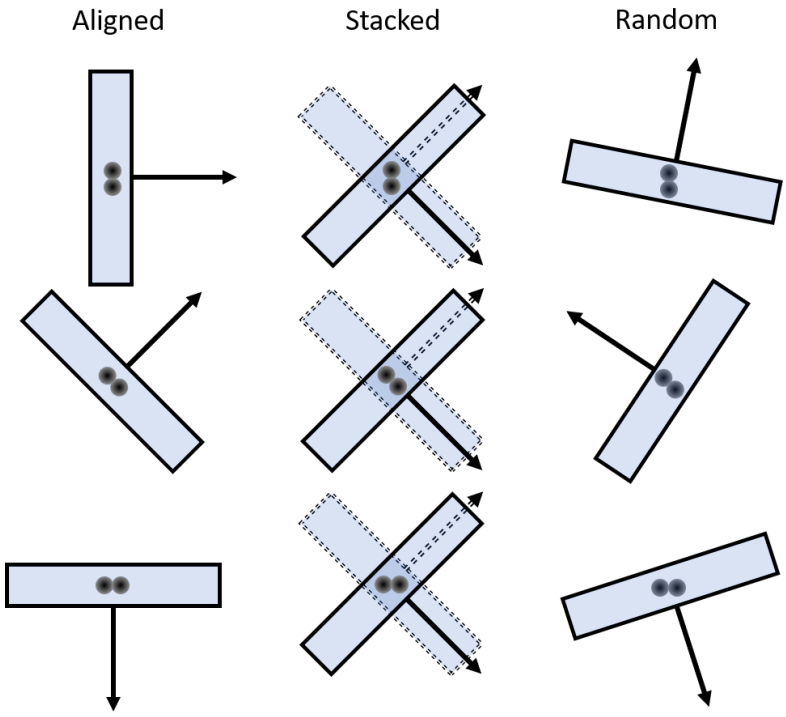

Figure 2: Observing scenarios. Arrows show spectral dispersion, circles show orientation of CSO, and rectangles show spectral window and orientation. **Left panel, aligned**: ideal spectrograph-CSO alignment provides a full strength position spectrum, but is unrealistic for detecting unknown CSOs.[1] **Center panel, stacked**: By capturing two frames with 90° field rotation between frames, the observer is guaranteed to capture the position spectrum of the event, although rarely at full strength. **Right panel, random**: with a single observation and no knowledge of the CSO event, an observer is at risk of occasionally missing the position spectrum of a CSO scenario entirely.

The position spectrum of closely spaced objects can be built up over long exposures, and thus is applicable to a wider range of brightness differences between targets, smaller telescopes, and so on, *so long as the exposure time required is short compared to the dynamics of relative motion between the observed objects.*

2.3 Convolutional Neural Networks

Convolutional neural networks provide both the broad support and inductive biases for computer vision problems.[?] This work adds to a growing body of work in computer vision for scientific imagery, in which authors find that convolutional neural networks are applicable to the high contrast imagery inherent to the field.

We utilize Residual Networks (ResNets), convolutional neural networks composed with skip connections and batch normalization for increased training speed and stability.[?] We tested ResNet-34 and ResNet-152, and adopted the ResNet-152 backbone despite the need for increased training based on improved performance.

We adopt the One Cycle learning rate schedule to improve training performance over standard, constant learning rates.[?]

3. THIS WORK

3.1 Mission Space

In pursuit of the proper sensing modalities for specific observing parameters (target, desired information, available observing equipment, site specifics, etc), it is necessary to clearly discuss the relative advantages of different methods for the detection of closely spaced objects. This can be difficult given that the three primary methods,

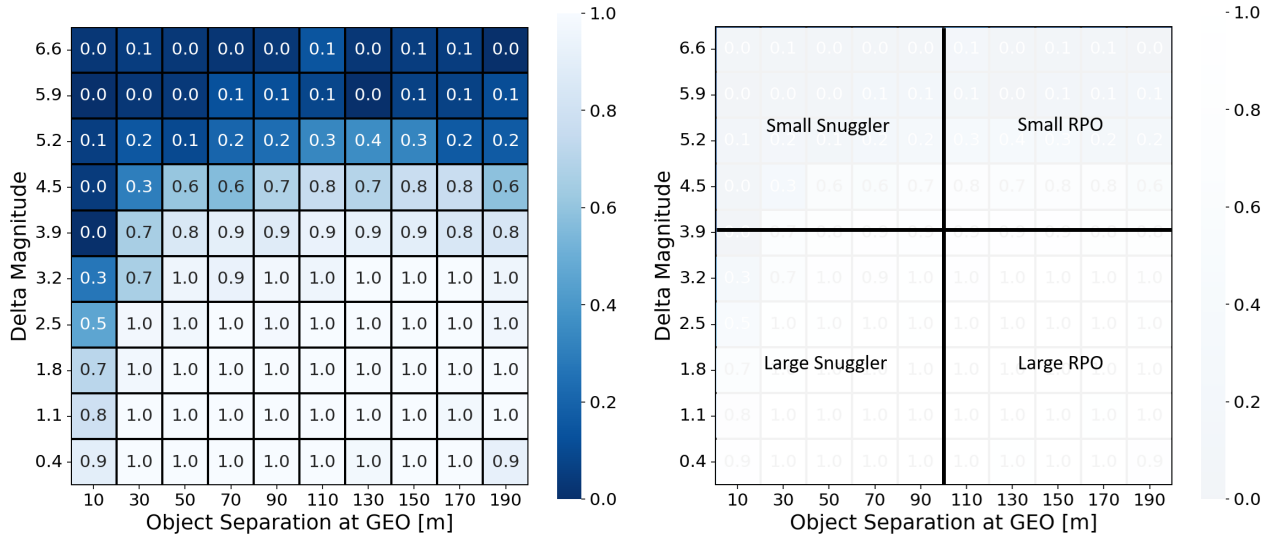

Figure 3: Visualization of model performance as a function of scenario dynamics. **Left panel; Separation vs. Relative Brightness**. The main parameters of interest for a CSO scenario are the separation of the objects in close proximity and the brightness difference between them. Each zone in the grid displays the overall CSO recall, from complete model failure at zero to ideal performance at one. Recall is chosen over accuracy as RSOs have no values for delta magnitude and object separation. In plots such as these, zero recall generally means that the model classifies all objects as single RSOs. Object separation along the x-axis is plotted in meters at GEO for easy consumption, but the less intuitive arcseconds of separation is applicable to objects at any distance. Delta magnitude is measured in astronomical magnitudes, a base $\sim$2.5 logarithmic scale in which a delta magnitude of one denotes a 2.5$\times$ difference in brightness. The ability to detect an secondary object significantly dimmer than the primary is of great interest to the astronomy community (exoplanets orbiting their host stars), and the space domain awareness community (where an unannounced object snuggling up to a high value asset could be quite small). **Right panel; Mission Design Space**. In this work we propose four areas for communicating cross-technique performance, as the overall classifier statistics in this space are enormously dependent on dataset parameters §5.3. In this panel we overlay the performance plot on the left with the mission geometries presented in this work.

Table 1: Simulated Dataset Parameters

Set	Parameter	Value
Atmosphere[??]	Seeing FWHM	U(0.4, 2.0)
	Airmass	U([1.0, 1.5, 2.0, 2.5, 3.0])
	PWV	0.5
	Observatory altitude [m]	3060
Instrument	Grating [grooves/mm, blaze]	150, 800
	Pixel Pitch [μm]	20
	Spectral resolution [nm]	6.5
	Dark Current [e^{-1}/ph/s]	0.005
	Read Noise [e^{-1} RMS]	3
	Bias [ADU/pix]	600
	PSF mode	Gaussian
	Gain	1.0
Scenario	visual magnitude m_v	U(10.0, 21.0)
	Δ m_v between CSOs	U(0.0, 8.0)
	CSO separation [arcseconds]	U(0.0, 1.15)
	CSO separation [meters]	U(0.0, 200.0)
	Orbit altitude [km]	36000

adaptive optics, speckle interferometry, and spectroastrometry rely on distinct observations of the underlying physics and observing conditions.

Because of this, shared datasets cannot be leveraged to assess differences between these techniques. This is problematic as overall classifier statistics (such as precision, recall, and accuracy used in this work) are highly dependent on the specifics of the dataset used. For example, if a dataset is observed in which all CSOs are separated on the ray of a telescope's observing direction, projected on sky CSO separation will always be zero and, thus, no technique is capable of discerning the presence of two objects.

Here we suggest a mission space vocabulary which divides the critical plane of relative brightness (measured in astronomical magnitudes) and object separation (measured in arcseconds, displayed in meters at geostationary orbit) into suggested scenarios which an operator may wish to probe.

In Fig. 9 we propose four regions of interest, small and large snuggler, and small and large rendezvous and proximity operation (RPO). The proposed distinction between small and large is, of course, relative to the brighter target, and we propose that small represent 4-7 magnitudes of difference between objects, while large represent 0-4 magnitudes of difference. We suggest that RPO scenarios occur between 100 and 200 meters of separation between targets, while a satellite "snuggling" up to another would remain within this, from 0 to 100 meters distance.

There are mission considerations which do not neatly fall into these categories, for example, an impact from tumbling debris might vary largely in delta magnitude as object separation shrinks to zero; however, such events would likely evolve so quickly as to make spectroastrometric characterization unnecessary.

3.2 Observing Modes

While prior work demonstrated the potential of spectroastrometry for space domain awareness,[1] that work was limited to simulations of ideal on sky alignment (see Fig. 1). Such alignment scenarios require a priori knowledge of the on sky geometry and, thus, knowledge of the existence of the CSO from another information source. As such, it is a useful application to the characterization of CSO scenarios but not to their detection.

In this work we extend the simulations of prior studies to include three observing modes: one in which the spectrograph and target scenario are ideally aligned, a second in which the spectrograph alignment is random with

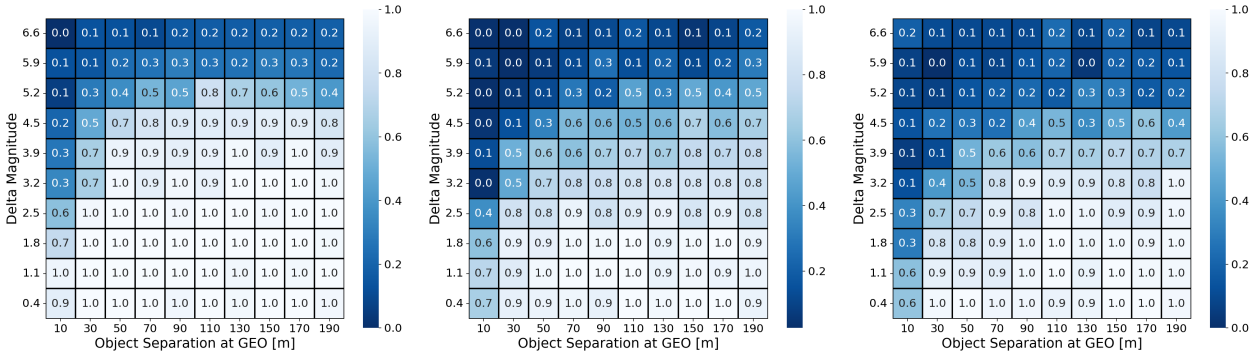

Figure 4: Classification trained on 2k examples. Mission space recall plots for CSOs in the test dataset evaluated on the trained classifier. **Left**; Aligned. **Center**; Stacked. **Right**; Random.

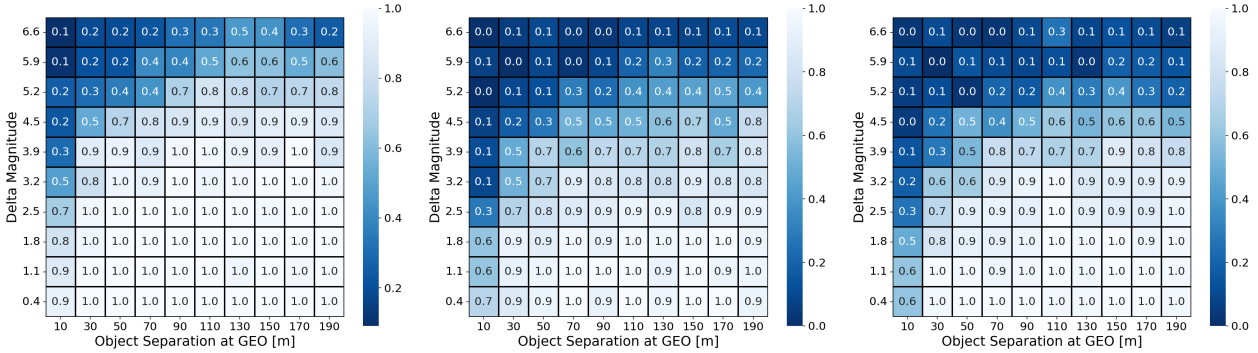

Figure 5: Classification trained on 10k examples. Mission space recall plots for CSOs in the test dataset evaluated on the trained classifier. **Left**; Aligned. **Center**; Stacked. **Right**; Random.

respect to the CSO, and a third which utilizes field rotation and double exposures to alleviate the weaknesses of random orientation without using a priori alignment information. The latter case, which we refer to as "Stacked" in this work, rotates the spectrograph field of view by 90° between two subsequent observations to remove the case of perfectly destructive alignment shown in Fig. 1.

These three modes−aligned, stacked, and random− are visualized in Fig. 2.

3.3 Characterization of Closely Spaced Objects

Joint classification and regression with a two headed output, one predicting one-hot encoded class vectors as in §5.1, and the second head regressing to four variables, separation between objects ($s_{''}$ [arcseconds] or s_m [meters]), difference in brightness $\Delta\ m_V$ (measured in astronomical magnitude), and two continuous variables representing on sky alignment of the CSO system, $\sin(\theta_{\text{CSO}})$ and $\cos(\theta_{\text{CSO}})$, where θ_{CSO} is referred to as the CSO position angle.

3.4 Instrumentation

We model the Spica-II spectrograph, built from commercial, off the shelf components and installed on the 3.6m AEOS telescope atop Haleakala. In simulation we modify the spectrograph to include field rotation via a K mirror, which allows high speed field rotation with minimal light loss and could be easily added to the compact instrument package of Spica-II.

4. DATASETS

Synthetic datasets in this work are modeled after the Spica-II spectrograph modified for field rotation (§3.4). We generate six training sets, combining 2000 or 10000 training examples (balanced between classes), and each of the three observing modes (aligned, stacked, and random) presented in §3.2.

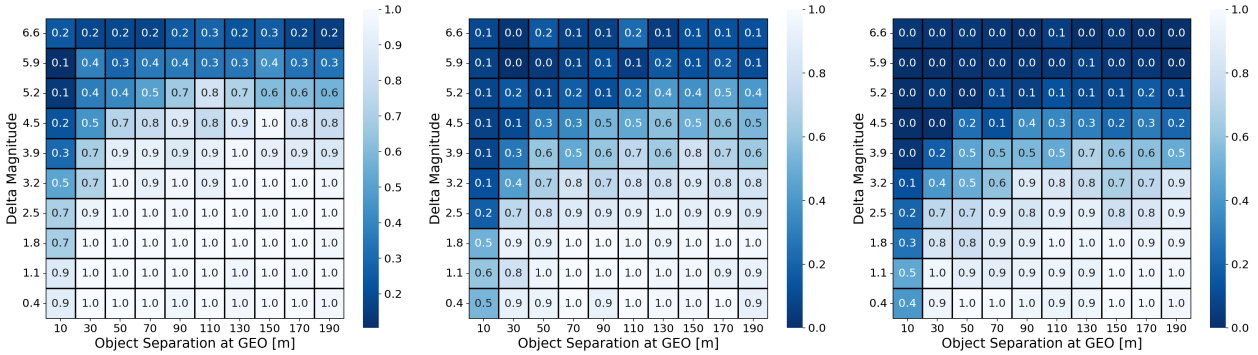

Figure 6: Joint classification and regression trained on 2k examples. Mission space recall plots for CSOs in the test dataset evaluated on the trained classifier. **Left**; Aligned. **Center**; Stacked. **Right**; Random.

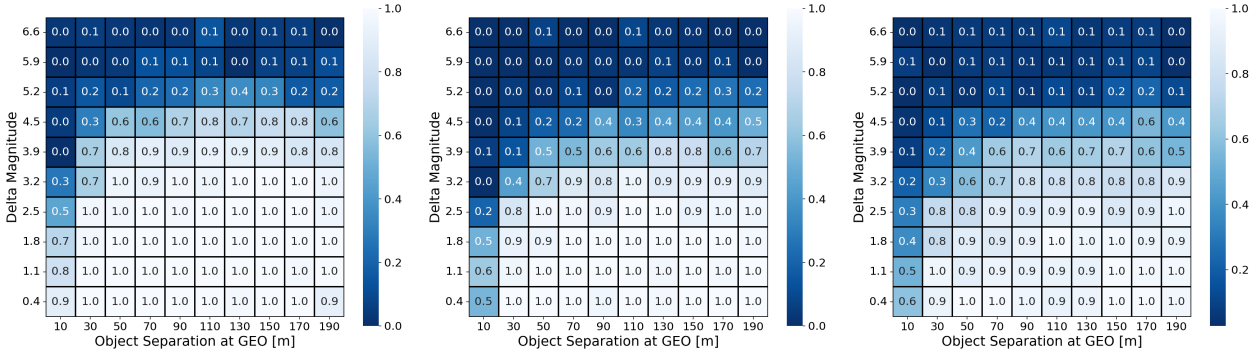

Figure 7: Joint classification and regression trained on 10k examples. Mission space recall plots for CSOs in the test dataset evaluated on the trained classifier. **Left**; Aligned. **Center**; Stacked. **Right**; Random.

Validation is performed using three 10000 balanced example sets corresponding to each mode, and three test sets of the same size are used only for the final plots and tables presented in this work.

Each dataset uses a version of SpecSim, a focal plane simulation tool for spectroscopic observations,[1] extended to handle random and stacked observing modes. The distributions of physical parameters from which each example is drawn are presented in Table 1.

5. EXPERIMENTS

The main mission driven parameters are the difference in brightness between the two objects (measured in astronomical magnitude), and the object separation, measured as an angular separation in arcseconds, which we plot and tabulate as meters of separation at geostationary orbit.

Experiments are conducted across multiple training dataset sizes, modeling methodologies, and observing modes. We discuss results as a function of modeling methodologies, separating into pure classification and joint regression with classification. For comparison purposes, both sections utilize ResNet-152 backbones for feature extraction, and all models are trained from random weight initialization. Error bars represent the stochastic scatter among five iterations run per model instantiation.

In classification problems, precision, recall, and F_1 score are calculated *per class*, while classifier accuracy is calculated across the entire dataset.

Statistic	Observing Scenario					
	Aligned		Stacked		Random	
	RSO	CSO	RSO	CSO	RSO	CSO
Classification Performance						
Precision	0.84 ± 0.08	0.66 ± 0.07	0.95 ± 0.03	0.43 ± 0.05	0.81 ± 0.05	0.51 ± 0.08
Recall	0.71 ± 0.02	0.82 ± 0.06	0.63 ± 0.02	0.90 ± 0.04	0.63 ± 0.02	0.73 ± 0.03
F_1	0.77 ± 0.02	0.73 ± 0.02	0.76 ± 0.01	0.58 ± 0.04	0.70 ± 0.01	0.60 ± 0.05
Accuracy	0.75 ± 0.01		0.69 ± 0.01		0.66 ± 0.02	

Table 2: Classification ResNet 152 backbone with 2k training examples balanced between single satellite and closely spaced objects.

Statistic	Observing Scenario					
	Aligned		Stacked		Random	
	RSO	CSO	RSO	CSO	RSO	CSO
Classification Performance						
Precision	0.86 ± 0.08	0.68 ± 0.07	0.88 ± 0.07	0.54 ± 0.05	0.86 ± 0.03	0.55 ± 0.04
Recall	0.73 ± 0.03	0.84 ± 0.07	0.66 ± 0.01	0.83 ± 0.06	0.66 ± 0.01	0.80 ± 0.03
F_1	0.79 ± 0.02	0.75 ± 0.02	0.75 ± 0.02	0.65 ± 0.02	0.75 ± 0.01	0.65 ± 0.02
Accuracy	0.77 ± 0.00		0.71 ± 0.01		0.71 ± 0.01	

Table 3: Classification ResNet 152 backbone with 10k training examples balanced between single satellite and closely spaced objects.

5.1 Threat identification via Classification

In operational space domain awareness, the detection of an unknown CSO scenario provides visibility into a rare but risky on orbit scenario. To assess the ability of spectroastrometry for CSO detection, we investigated the application of simple binary classification via ResNet-152 with a softmax classification head to the problem of CSO detection. The results of these experiments are tabulated in Tbls 2 & 3, appear graphically in Figs 4 & 5, and accuracies are compared with all other methodologies in Fig. 8.

As expected, we find that knowledge of the CSO's position angle significantly improves classifier performance. For realistic applications of this sensing modality to CSO *detection*, however, we fall either into the case of a single randomly aligned exposure, or a double exposure with a 90° field rotation. Here we show that stacking field-rotated frames does marginally improve detector sensitivity. This is to be expected, as field rotation removes the chance of chance destructive alignments which make CSO detection impossible (see, for example, Fig.1).

5.2 Scenario investigation with Regression

Ideally, a technique used to detect CSOs would also provide characterizing information about the on orbit scenario itself. We design a joint classification regressor which provides softmax classification while regressing to four variables, separation between objects ($s_{''}$ [arcseconds] or s_m [meters]), difference in brightness $\Delta\ m_V$(measured in astronomical magnitude), and two continuous variables representing on sky alignment of the CSO system, $\sin(\theta_{\mathrm{CSO}})$ and $\cos(\theta_{\mathrm{CSO}})$, where θ_{CSO} is referred to as the CSO position angle.

Results of these experiments are tabulated in Tbls 4 & 5, appear graphically in Figs 6 & 7, and accuracies are compared with all other methodologies in Fig. 8.

We again find that models with ideal spectrograph alignment outperform all others in classification accuracy, while stacked field rotated frames marginally outperform random alignments. Performance dropped slightly with respect to pure classification models, despite our expectations that regression would serve as an auxillary task.

Statistic	Observing Scenario					
	Aligned		Stacked		Random	
	RSO	CSO	RSO	CSO	RSO	CSO
Classification Performance						
Precision	0.83 ± 0.08	0.65 ± 0.08	0.87 ± 0.11	0.48 ± 0.15	0.85 ± 0.12	0.48 ± 0.08
Recall	0.71 ± 0.03	0.80 ± 0.07	0.63 ± 0.04	0.83 ± 0.14	0.62 ± 0.00	0.79 ± 0.15
F_1	0.76 ± 0.02	0.71 ± 0.02	0.73 ± 0.01	0.59 ± 0.10	0.71 ± 0.04	0.59 ± 0.03
Accuracy	0.74 ± 0.00		0.68 ± 0.02		0.66 ± 0.02	
Regression Mean Absolute Errors						
θ_{CSO}	–	89.80 ± 0.41	–	61.09 ± 4.15	–	66.95 ± 4.46
Δm_V	–	0.96 ± 0.04	–	1.26 ± 0.09	–	1.26 ± 0.05
$s_{//}$	–	0.28 ± 0.00	–	0.28 ± 0.00	–	0.29 ± 0.01
s_m	–	49.11 ± 0.37	–	49.13 ± 0.68	–	50.37 ± 1.53

Table 4: Joint regression with classification ResNet 152 backbone with 2k training examples balanced between single satellite and closely spaced objects. Single satellite RSOs have no associated regression variables as defined in this work.

In our datasets, the expected mean absolute error (MAE) for random guessing is $\theta_{CSO} = 90°$. We find that the aligned scenarios provide no information on the CSO alignment, as expected: while perfectly aligned, no information about on sky orientation flows through gradients during training. Surprisingly, regression to θ_{CSO} in stacked frames provided only slightly decreased MAE than iterating on random frames, where the spectrograph slit is oriented at a constant zero degrees. We hypothesize that frame stacks with additional rotations would further decrease θ_{CSO} MAE.

Statistic	Observing Scenario					
	Aligned		Stacked		Random	
	RSO	CSO	RSO	CSO	RSO	CSO
Classification Performance						
Precision	0.88 ± 0.03	0.64 ± 0.02	0.87 ± 0.03	0.56 ± 0.03	0.96 ± 0.05	0.41 ± 0.05
Recall	0.71 ± 0.00	0.84 ± 0.03	0.66 ± 0.01	0.81 ± 0.03	0.62 ± 0.01	0.92 ± 0.09
F_1	0.79 ± 0.01	0.73 ± 0.00	0.75 ± 0.01	0.66 ± 0.01	0.75 ± 0.01	0.56 ± 0.03
Accuracy	0.76 ± 0.01		0.71 ± 0.00		0.68 ± 0.01	
Regression Mean Absolute Errors						
θ_{CSO}	–	90.01 ± 0.23	–	44.69 ± 0.81	–	67.50 ± 7.67
Δm_V	–	0.90 ± 0.02	–	1.08 ± 0.05	–	1.28 ± 0.09
$s_{//}$	–	0.28 ± 0.00	–	0.27 ± 0.00	–	0.29 ± 0.01
s_m	–	49.06 ± 0.23	–	47.75 ± 0.35	–	49.94 ± 1.70

Table 5: Joint regression with classification ResNet 152 backbone with 10k training examples balanced between single satellite and closely spaced objects. Single satellite RSOs have no associated regression variables as defined in this work

5.3 Mission Space Performance Statistics

To enable comparison with alternate CSO detection techniques, or spectroastrometric results evaluated on different datasets, we present our results in a dataset independent format. In Sections 5.1-5.2, reported classification and regression statistics are dependent largely on the parameter spread (and thus "difficulty") of the dataset used. For example, performance statistics on a test dataset which contains delta magnitudes between 0 and 5 will be significantly better than that of a dataset between 0 and 10. Because of this, we propose a mission space decomposition with the significant components delta magnitude and object separation (§3.1, Fig. 9).

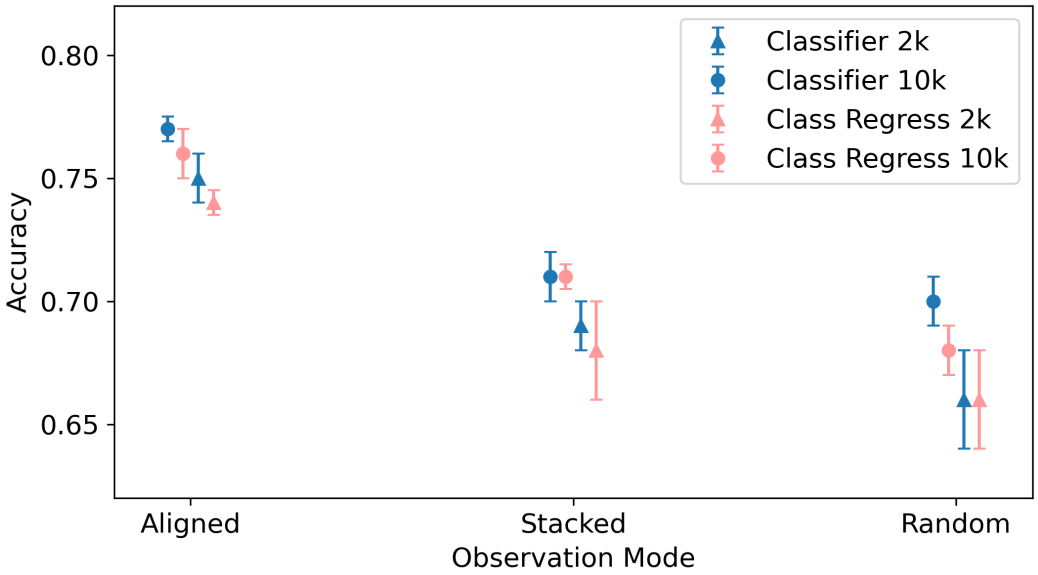

Figure 8: Accuracy across model backbone and training dataset sizes. Accuracy is plotted against observing mode, with blue points representing curves from classifiers and red representing regression with classification. Circles denote 10k datasets while triangles show 2k datasets. While a priori knowledge of CSO alignment allowing for aligned observations significantly outperforms other scenarios, a modest boost due to stacked observations shows that removing destructive alignment scenarios is useful in practice.

Mission Space	Statistics					
	Classification			Regression		
	Precision	Recall	F_1	θ_{CSO}	Δm_V	s_m
Spectrograph Aligned with Scenario (Accuracy = 0.74 ± 0.00)						
RSO	0.83 ± 0.08	0.71 ± 0.03	0.76 ± 0.02	–	–	–
CSO	0.65 ± 0.08	0.80 ± 0.07	0.71 ± 0.02	89.80 ± 0.41	0.96 ± 0.04	49.11 ± 0.37
Large RPO	0.91 ± 0.04	1.00 ± 0.00	0.95 ± 0.02	89.60 ± 0.76	0.82 ± 0.03	47.51 ± 4.40
Large Snuggler	0.83 ± 0.06	0.76 ± 0.13	0.78 ± 0.04	88.75 ± 0.25	1.22 ± 0.01	49.41 ± 3.85
Small RPO	0.41 ± 0.12	1.00 ± 0.00	0.58 ± 0.11	90.58 ± 0.75	0.89 ± 0.09	59.23 ± 2.15
Small Snuggler	0.33 ± 0.12	0.44 ± 0.02	0.37 ± 0.08	90.64 ± 0.97	0.89 ± 0.09	41.30 ± 1.93
Stacked Field Rotated Frames (Accuracy = 0.68 ± 0.02)						
RSO	0.87 ± 0.11	0.63 ± 0.04	0.73 ± 0.01	–	–	–
CSO	0.48 ± 0.15	0.83 ± 0.14	0.59 ± 0.10	61.09 ± 4.15	1.26 ± 0.09	49.13 ± 0.68
Large RPO	0.77 ± 0.13	0.77 ± 0.20	0.75 ± 0.02	45.47 ± 4.66	1.18 ± 0.22	38.12 ± 3.15
Large Snuggler	0.59 ± 0.17	0.98 ± 0.01	0.73 ± 0.14	57.33 ± 3.55	1.71 ± 0.28	59.61 ± 5.57
Small RPO	0.26 ± 0.18	0.75 ± 0.21	0.34 ± 0.21	70.24 ± 4.48	1.06 ± 0.16	49.39 ± 4.84
Small Snuggler	0.16 ± 0.12	0.88 ± 0.07	0.26 ± 0.19	78.15 ± 4.24	0.99 ± 0.12	50.46 ± 4.75
Random Spectrograph Alignment (Accuracy = 0.66 ± 0.02)						
RSO	0.85 ± 0.12	0.62 ± 0.00	0.71 ± 0.04	–	–	–
CSO	0.48 ± 0.08	0.79 ± 0.15	0.59 ± 0.03	66.95 ± 4.46	1.26 ± 0.05	50.37 ± 1.53
Large RPO	0.76 ± 0.04	1.00 ± 0.00	0.86 ± 0.03	56.85 ± 3.03	1.15 ± 0.08	60.40 ± 7.85
Large Snuggler	0.59 ± 0.06	0.65 ± 0.25	0.60 ± 0.08	59.96 ± 3.50	1.49 ± 0.09	37.37 ± 5.27
Small RPO	0.23 ± 0.11	1.00 ± 0.00	0.37 ± 0.15	75.49 ± 6.97	1.20 ± 0.21	70.12 ± 7.81
Small Snuggler	0.20 ± 0.12	0.67 ± 0.23	0.28 ± 0.15	81.22 ± 5.45	1.17 ± 0.22	34.61 ± 4.32

Table 6: Mission space performance for joint regression and classification on the 2k dataset.

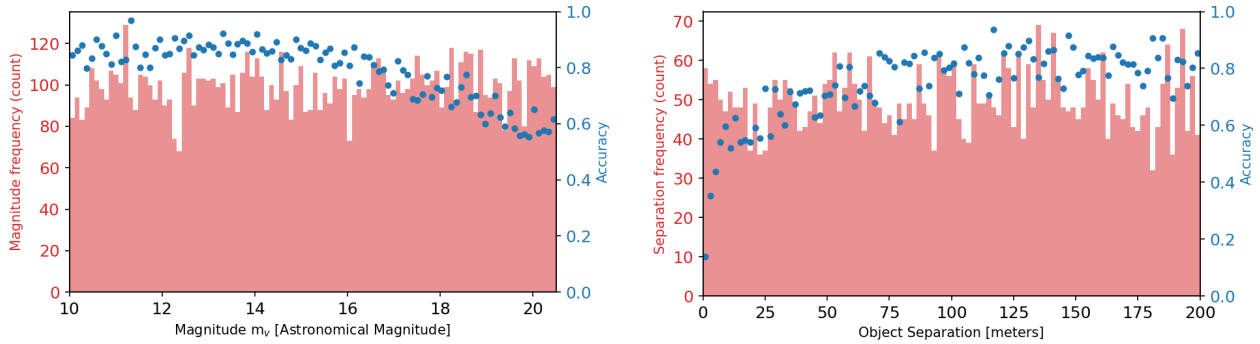

Figure 9: Accuracy with respect to physical parameters. Plotted for the best overall performing model (10k training set, aligned classifier of Table 3), these figures demonstrate the evolution of accuracy with respect to physical parameters of the observed system. **Left panel**; target magnitude. This shows a decrease in global performance as magnitude increases (and, thus, brightness decreases), a result of instrument sensitivity and telescope collecting area. **Right panel**; object separation. As expected, when the separation between objects decreases, so does classifier accuracy.

We present these results for our joint regression with classification models in Tbls 6 and 7 for 2k and 10k datasets, respectively.

Mission Space	Statistics					
	Classification			Regression		
	Precision	Recall	F_1	θ_{CSO}	Δm_V	s_m
Spectrograph Aligned with Scenario (Accuracy = 0.76 ± 0.01)						
RSO	0.88 ± 0.03	0.71 ± 0.00	0.79 ± 0.01	–	–	–
CSO	0.64 ± 0.02	0.84 ± 0.03	0.73 ± 0.00	90.01 ± 0.23	0.90 ± 0.02	49.06 ± 0.23
Large RPO	0.94 ± 0.00	0.81 ± 0.03	0.87 ± 0.02	89.56 ± 0.46	0.74 ± 0.07	43.33 ± 6.38
Large Snuggler	0.84 ± 0.02	0.93 ± 0.10	0.88 ± 0.04	89.92 ± 0.86	1.18 ± 0.06	54.20 ± 6.09
Small RPO	0.36 ± 0.03	0.88 ± 0.13	0.51 ± 0.04	91.33 ± 1.16	0.82 ± 0.03	52.61 ± 1.43
Small Snuggler	0.26 ± 0.03	0.71 ± 0.11	0.38 ± 0.02	89.46 ± 0.52	0.83 ± 0.02	46.89 ± 1.58
Stacked Field Rotated Frames (Accuracy = 0.71 ± 0.00)						
RSO	0.87 ± 0.03	0.66 ± 0.01	0.75 ± 0.01	–	–	–
CSO	0.56 ± 0.03	0.81 ± 0.03	0.66 ± 0.01	44.69 ± 0.81	1.08 ± 0.05	47.75 ± 0.35
Large RPO	0.88 ± 0.01	0.99 ± 0.01	0.93 ± 0.00	22.78 ± 1.76	0.96 ± 0.12	38.90 ± 0.84
Large Snuggler	0.71 ± 0.01	0.80 ± 0.17	0.75 ± 0.08	33.88 ± 0.96	1.41 ± 0.04	53.47 ± 2.23
Small RPO	0.29 ± 0.07	0.75 ± 0.30	0.40 ± 0.08	60.37 ± 2.41	0.97 ± 0.07	60.46 ± 5.39
Small Snuggler	0.19 ± 0.06	0.54 ± 0.11	0.28 ± 0.05	72.91 ± 0.91	0.91 ± 0.04	40.42 ± 3.71
Random Spectrograph Alignment (Accuracy = 0.68 ± 0.01)						
RSO	0.96 ± 0.05	0.62 ± 0.01	0.75 ± 0.01	–	–	–
CSO	0.41 ± 0.05	0.92 ± 0.09	0.56 ± 0.03	67.50 ± 7.67	1.28 ± 0.09	49.94 ± 1.70
Large RPO	0.73 ± 0.05	0.96 ± 0.07	0.83 ± 0.01	57.69 ± 8.33	1.23 ± 0.23	52.94 ± 12.75
Large Snuggler	0.53 ± 0.05	0.95 ± 0.05	0.68 ± 0.04	60.55 ± 8.65	1.71 ± 0.27	43.83 ± 10.37
Small RPO	0.13 ± 0.06	0.82 ± 0.32	0.21 ± 0.08	76.28 ± 7.58	1.04 ± 0.14	66.59 ± 14.35
Small Snuggler	0.08 ± 0.05	0.82 ± 0.05	0.15 ± 0.08	81.13 ± 5.98	1.01 ± 0.12	37.89 ± 10.87

Table 7: Mission space performance for joint regression and classification on the 10k dataset.

6. CONCLUSIONS

In this work we refine a proposed method of spectroastrometry for detection and characterization of closely spaced objects in geostationary orbit[1] by removing the need for a priori knowledge of CSO on sky orientation. We show that our technique improves classification accuracy over the more common random orientation case, and demonstrate regression to the variables defining the CSO scenario.

The rare occurrence of high-risk CSO scenarios renders difficult the collection of large, balanced training sets. In studies of CSO detection via speckle interferometry, datasets on single and binary stars offer an intriguing analog to isolated and closely spaced artificial satellites. In spectroastrometry, the analog is harder to justify, as both artificial satellites are illuminated by the same sunlight, imparting differences in reflection based on specifics of the satellites. While we know these differences are enough to identify objects,[4] they are quantitatively different to spectral differences between the emission spectra of binary stars.

While binary asteroids would serve as a better proxy for both speckle interferometry and spectroastrometry, systems that are bright enough with proper ground truth observations for labeling magnitudes, separations, orientations, and delta magnitudes are few and far between.

We recommend instead that future work focus on alternate methods to reduce the burden of data collection. It may be fruitful, for example, to reformulate this problem as a one-class classifier with outlier detection or to investigate the applicability of domain adaptation from simulated data to real to balance the training dataset. Here the growing datasets of RSOs from studies like[4] would provide useful training data.

This technique might add additional value to spectroscopic analysis of large satellites at GEO, where regression to on sky angle might aid in the refinement of orbital pose[6] by, say, detecting on sky alignment of large solar panels or communication arrays.

REFERENCES

[1] Gazak, J., Swindle, R., Mcquaid, I., and Fletcher, J., "Exploiting Spatial Information in Raw Spectroscopic Imagery using Convolutional Neural Networks," (Sept. 2020).

[2] Bailey, J. A., "Spectroastrometry: a new approach to astronomy on small spatial scales," in [*Optical Astronomical Instrumentation*], **3355**, 932–939, SPIE (July 1998).

[3] Whelan, E. and Garcia, P., "Spectro-astrometry: The Method, its Limitations, and Applications," (2008).

[4] Gazak, J. Z., McQuaid, I., Swindle, R., Phelps, M., and Fletcher, J., "SpectraNet: Learned Recognition of Artificial Satellites from High Contrast Spectroscopic Imagery," *WACV* , 9 (2022).

[5] Gazak, J., Mcquaid, I., Wolfson, B., and Fletcher, J., "Incremental Learning of Novel Resident Space Object Spectral Fingerprints," (Sept. 2021).

[6] Phelps, M., Gazak, J., Swindle, T., Mcquaid, I., and Fletcher, J., "Inferring Space Object Orientation with Spectroscopy and Convolutional Networks," (Sept. 2021).

[7] Fletcher, J., Mcquaid, I., Thomas, P., Sanders, J., and Martin, G., "Feature-Based Satellite Detection using Convolutional Neural Networks," (Sept. 2019).